Gel-Free Electrophoresis of DNA and Proteins on Chips Featuring a 70 nm Capillary–Well Motif

Zhen Cao and Levent Yobas*

Department of Electronic and Computer Engineering, Hong Kong University of Science and Technology, Clear Water Bay, Kowloon, Hong Kong

ABSTRACT We present an integrated glass capillary system on silicon for size-based sieving of distinct mixtures of proteins, short DNA, and long DNA fragments into sharp peaks. The minimum resolvable size difference achieved is noted as 3.45 kDa for 45–52.8 kDa proteins, 20 bp for 200–300 bp DNA strands, and 182 bp for 5.6–5.8 kbp DNA chains. This high-resolution sieving arises from vastly steep entropic barriers created at the onsets of extremely restrictive (resistive) capillary segments and their pivotal role in shifting the equilibrium entropic sieving to intense fields (>1000 V/cm). DNA fragments of various sizes are shown fully resolved in less than 7 min at a steady voltage of 2000 V being directly applied across the length of a 2 cm long sieve featuring thousands of entropic barriers. The utility of higher field strengths and longer sieves is also demonstrated without triggering dielectric breakdown by time-division multiplexing up to 2000 V across the 1 cm long sieve segments. The self-enclosed 70 nm diameter capillaries were fabricated using coarse (>1 μm) photolithography and standard semiconductor manufacturing techniques.

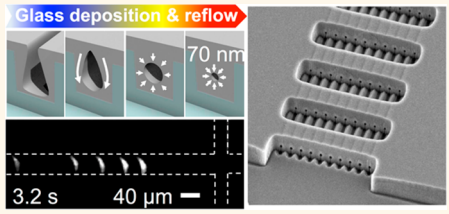

KEYWORDS: nanocapillary · DNA · proteins · separation · nanofabrication · nanofluidics

Advancing the fields of molecular biology, proteomics, and genomics is closely intertwined with the development of modern techniques that can be used to sieve biomolecules at increasingly high resolution and speeds.[1] DNA molecules, for instance, are typically separated using gel electrophoresis, but separation efficiency deteriorates in the case of fragments longer than ~20 kbp.[2] Although chains considerably longer than this can be resolved after making modest alterations to the method (*i.e.*, pulsed-field gel electrophoresis), the process is slow and the recovery of the separated molecules from gel is inefficient. A radical approach involves replacing conventional gels with artificial periodic-pore structures, and this has been demonstrated to be more effective than the traditional approach.[3] Since the pioneering work of Austin,[4] a host of such structures has been proposed, including post arrays,[4–10] colloidal crystals,[11] and arrays of alternating slits and wells (the slit–well motif).[12–17] However, the resolving power of some of these structures remains limited mostly because of insufficient sieve length, which is caused by the short spatial extent of advanced patterning or self-assembly techniques.[18]

The slit–well motif, which features entropic barriers, has attracted considerable attention not only because of its simple design, which can be patterned using standard photolithography, but also because of its moderately decent resolving power.[12–17] This is largely because entropic barriers at slit–well interfaces stop the diffusion of molecules across slits before it becomes a major source of dispersion.[14] To concurrently increase separation resolution and speed, electric field strengths and sieve lengths must be increased. However, in the slit–well motif, high electric fields (≳100 V/cm) cause the entropic sieving mechanisms (Supporting Information) to breakdown and thus result in an inevitable loss of resolving power.[15,17] Herein, using distinct mixtures of proteins and DNA fragments, we demonstrate that these entropic sieving mechanisms can be shifted to markedly higher fields (≳1000 V/cm) than those used before by adopting vastly steep entropic barriers; consequently, the resolution is enhanced and the effective runtime is concomitantly cut down (for detailed benchmarking, refer

* Address correspondence to eelyobas@ust.hk.

Received for review October 1, 2014 and accepted December 23, 2014.

Published online December 23, 2014
10.1021/nn505605e

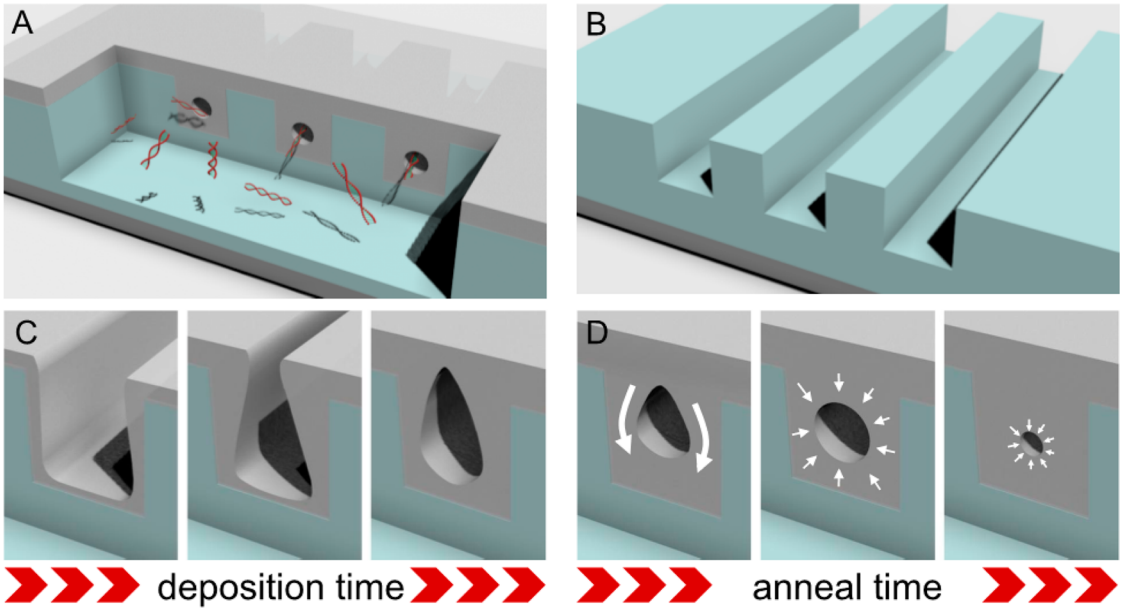

Figure 1. (A) Three-dimensional rendering of an integrated capillary−well region. (B−D) Fabrication steps: (B) lithographic engraving of coarse trench features (>1 μm) for use as a template for precision molding the cylindrical glass capillaries; (C) deposition of a doped glass layer and the formation of self-enclosed capillaries as the layer grows to "pinch off" trench openings due to nonconformal step coverage; (D) reflow of the doped glass layer during thermal annealing and shape transformation within trenches through which capillaries evolve into cylindrical tubes. Extending the annealing time reduces the capillary diameter. The arrows indicate the thermal reflow of doped glass.

to Supporting Information text and Table S1). (The effective runtime refers to the net time during which bands actively migrate through the sieve under a steady voltage, and it excludes the idle intervals introduced by time-division multiplexing the applied voltage.) This is achieved by simply replacing the slits (1D confinement) with capillaries (2D confinement). The capillary−well motif presented here consists of a set of integrated cylindrical glass capillaries that are 70 nm in nominal diameter. Using this sieve, biomolecules over a broad size range can be fully resolved under 7 min. Notably, the fabrication of such capillaries does not require advanced lithography techniques: it relies on a thermal reflow of doped glass within coarsely patterned trenches (>1 μm), which transforms the buried voids into cylindrical tubes (Figure 1).[19−21] More importantly, the capillary diameter can be shrunk uniformly by extending the annealing duration.[22] This method of fabrication differs from previous methods of constructing nanometer-scale (nanoscale) channels for handling DNA molecules, although it similarly leverages the shadowing-based deposition.[23−29] For instance, Cao *et al.* showed self-enclosed channels as small as 10 nm by 50 nm by exploiting nonuniform deposition techniques to further narrow and seal nanochannels (<100 nm).[23] Alternatively, Xia *et al.* obtained 9 nm channels by ultrafast laser pulse melting silicon to enclose nanochannels and then self-limiting thermal oxidation to further shrink the channel sizes.[27] Li *et al.* rather used a low-temperature process compatible with active elements and metals and demonstrated self-enclosed channels down to 100 nm width based on sacrificial layer removal.[24] In these methods, various techniques were used, such as nanoimprint[23−27] or interference lithography[28] or focused ion-beam milling.[29]

RESULTS AND DISCUSSION

Sieve Structure. Figure 2A shows a scanning electron micrograph of a representative sieve after a key fabrication step; the image is focused on the sample-injection cross-junction and the first few units of the capillary−well array. An enlarged view of the first capillary−well unit is presented in Figure 2B. The capillary openings are highly regular and are approximately 750 nm in diameter as a result of the initial thermal annealing performed before structuring the wells and the sample-injection cross-junction. A subsequent application of additional thermal annealing transformed the capillaries into nanoscale tubes. Figure 2C shows a cross-sectional view of the capillaries. Remarkably, after the capillaries shrink in diameter by an order of magnitude to d_c = 70 nm, their cross-sectional profile remains highly regular (Figure 2D).

The capillary diameter, d_c, plays a determining role in the sieving dynamics of molecules. Because the d_c value obtained was *not* a direct consequence of a lithographic patterning or precision etching process, we investigated its potential variation across batches. Three designs featuring distinct pitch sizes, 4, 10, and 20 μm, all from the same batch, yielded values of 73.9 $\pm$ 4.1, 72.3 $\pm$ 3.1, and 70.7 $\pm$ 3.0 nm, respectively; these mean $\pm$ SD values were obtained by evaluating 10 capillaries from each design across random cuts

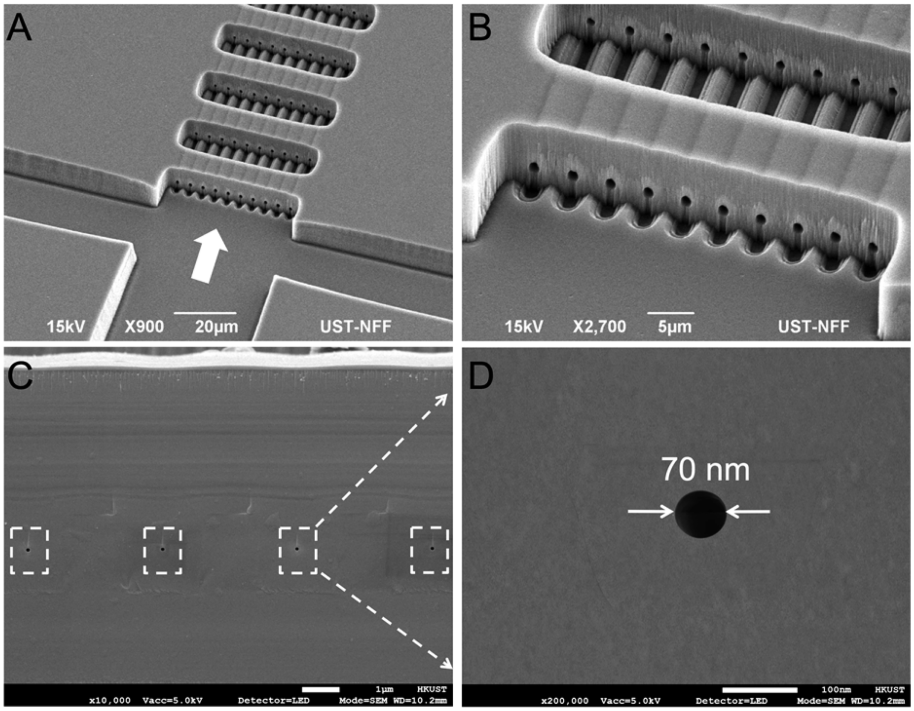

Figure 2. Scanning electron micrographs of a representative sieve that featured a capillary−well pitch size L_u = 20 μm. (A) Close-up view of the sample-injection cross-junction and (B) first capillary−well unit; both images were obtained after the first thermal annealing step that led to the reflow and transformed the capillaries into 750 nm diameter cylindrical tubes. The wells and the sample-injection cross-junction were then structured. (C,D) Micrographs obtained of the same device after additional thermal annealing was applied, which scaled the capillary diameter further down to d_c = 70 nm. Scale bars: (A) 20, (B) 5, (C) 1 μm, and (D) 100 nm.

along the sieve. Further evaluations of designs featuring the aforementioned pitch sizes in subsequent batches yielded values of 75.6 ± 4.1, 73.1 ± 3.4, and 70.2 ± 1.3 nm in one batch and 74.6 ± 3.2, 72.4 ± 2.5, and 70.4 ± 1.4 nm in another, respectively. All the devices were subjected to the same process steps as the rest of the devices presented herein and were determined to exhibit a relative standard deviation of <6%. This consistency is outstanding given that their diameter is in the nanoscale range (<100 nm) over a high aspect ratio (length/diameter up to ~150) and, above all, that they were fabricated using conventional photolithography.

Another key design feature is the period or pitch size, L_u, of the array. In the device shown here, the pitch is 20 μm and the sieving matrix extends over a separation length, L_s, of 2 cm and contains 1000 nearly identical repeating units, the entropic traps (N_{trap}). We also tested designs that featured comparatively finer pitches (4 and 10 μm) and thus contained more entropic traps (5000 and 2000). In all the designs, the pitch was equally divided between a well (42 μm wide, 6 μm deep) and a set of 10 identical parallel capillaries (d_c = 70 nm). In certain designs, the periodic sieving matrix was 3 cm long.

Sieving Short DNA. Figure 3A shows the electrophoretic separation of a 100 bp DNA ladder in a 70 nm capillary−well array that featured a pitch of 4 μm and was 2 cm long (N_{trap} = 5000). When an average field of E_{av} = 1000 V/cm was established through a steady 2000 V directly applied across the entire sieve length, the strands were separated in <5 min into single peaks based on their size, with smaller strands migrating at a higher mobility (Ogston sieving). The resolution values, R_s, typically exceeded 3, and the theoretical plate numbers were 1−2 × 10^4 (up to 10^6 plates/m). The resolution between peaks 200 and 300 bp was particularly notable, R_s = 5.05, indicating a minimum resolvable size difference of R_M = 20 bp, which was estimated using the differential size of two peaks, ΔM, and the relation $R_M = \Delta M/R_s$. By comparison, a baseline separation of a 100 bp DNA ladder (R_M = 67 bp) in an 80 nm slit−well array that featured the same period but half the array length required 2.5 h under an average field of $E_{av} \sim 26$ V/cm.[17] Under an average field of $E_{av} \gtrsim 100$ V/cm, Ogston sieving in the slit−well design became ineffective. The capillary−well array not only maintained a quasi-equilibrium sieving mode at E_{av} = 1000 V/cm but also required such intense fields in order to facilitate band launching. The launching of bands in the reported device failed when the field strength was slightly below E_{av} = 1000 V/cm. The requirement of a high-field threshold for launching samples is a hallmark of the highly restrictive capillary−well motif that was first reported in our previous design in which we used larger capillaries (diameter, 750 nm; pitch, 45 μm) than those used here, and thus the previous design was suitable only for sieving long chains.[21] Despite the high-field threshold, the corresponding field strength within the wells was

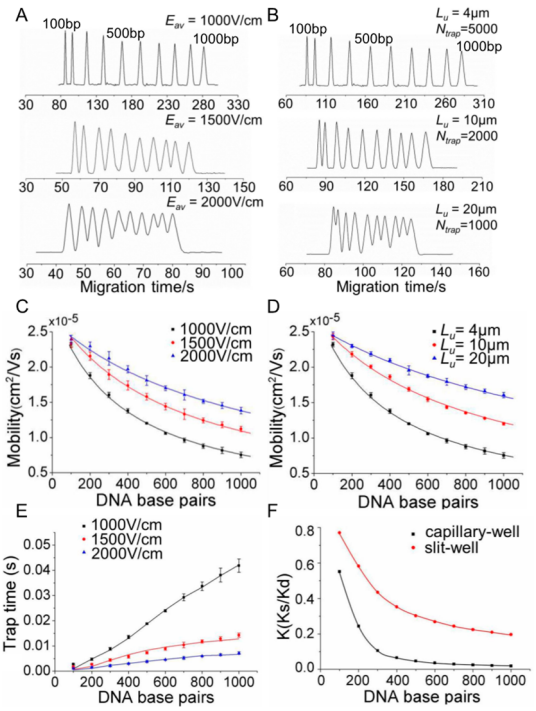

Figure 3. Electrophoretic separation of a 100 bp DNA ladder. Electropherograms obtained from (A) the same design (L_u = 4 μm; d_c = 70 nm; L_s = 2 cm) under distinct field strengths and (B) separate designs (d_c = 70 nm; L_s = 2 cm) featuring distinct pitch sizes (L_u) and numbers of entropic traps (N_{trap}), all under E_{av} = 1000 V/cm. Respective mobility plots (C,D) and a plot of the mean trapping time (E) are shown as a function of DNA size (n = 5). The partition coefficient K values (F) for the capillary−well motif and an equivalent slit−well motif.

fairly low, as discussed later, and this could explain the presence of such a distinct threshold for launching bands.

The molecular sieving power of the capillary−well array depended on the field and deteriorated with increasing driving-field intensity. As in the slit−well array, the field dependence of mobility was more apparent for longer chains than for shorter ones, further attesting that Ogston sieving was the dominant mechanism for sieving the 100 bp DNA ladder. Nevertheless, the capillary−well array exhibited a high capacity to handle intense fields: it can sustain an additional >500 V/cm, as opposed to the tens of volts per centimeter in a slit−well motif, before its sieving power deteriorates markedly.[16] Under E_{av} = 1500 V/cm, all strands could still be resolved relative to baseline, except for a slight overlap between 800 and 900 bp. Under 2000 V/cm, the separation resolution of long strands (>400 bp) deteriorated further, but the resolution of shorter strands was affected to a comparatively lesser extent. When the field was increased from 1000 to 2000 V/cm, the mobility of 1000 bp chains increased by 84%; this is considerably more pronounced than the 3% increase in the mobility of 100 bp strands. In all the runs, the electro-osmotic mobility was negligible because it was mostly quenched as a result of using a high ionic strength buffer (5× TBE).

The pitch of the capillary−well array sets the density of the entropic traps per unit length. When the pitch is increased for a given array length, molecules encounter a reduced number of entropic traps and thus the separation resolution deteriorates. Figure 3B shows this effect on the separation of a 100 bp DNA ladder under E_{av} = 1000 V/cm: the resolution and the number of theoretical plates worsened when the pitch was increased while maintaining a constant array length, and thus the number of entropic traps that molecules encountered was proportionally decreased (N_{trap} = 5000, 2000, and 1000 in designs featuring L_u = 4, 10, and 20 μm, respectively).

The mobility curves that were derived from the band-elution time, the migration distance, and the average electric-field strength are plotted in Figure 3C,D. In the plots, the solid lines represent the best fits to the data based on the model $\mu = \mu_{max}/(1 + AN)$, which involves the number of base pairs N and two fitting parameters specific to sieves: μ_{max}, the maximal sieving-free mobility, and A, the size selectivity.[21] Excellent agreement with the data was obtained for all the curves ($R^2 \geq 0.99$), and the optimal fitting values were $\mu_{max} \sim 2.8 \times 10^{-5}$ cm^2/Vs and $A \sim 0.6-2.9 \times 10^{-3}$. Whereas μ_{max} varied little among the curves, A increased with an increase in the number of entropic traps and/or a decrease in the average field strength. When the A value increased, the size selectivity was also enhanced; this is because the slope of the mobility curve, $d\mu/dN(N \rightarrow 0)$, is an increasing function of A and a high slope reflects high selectivity. Thus, optimal selectivity was obtained when the curve was the steepest, which was in the case of the curve for the maximum number of entropic traps (N_{trap} = 5000 and L_u = 4 μm) and the minimum possible field strength above the threshold (E_{av} = 1000 V/cm).

Figure 3E shows the trapping time of the molecules at a capillary entrance (entropic barrier) that was calculated directly from the experimental mobility values (Figure 3C) by using

$$\tau_{trap} = \tau_m\left(\frac{\mu_{max}}{\mu} - 1\right) \quad (1)$$

where the drift time of the molecules between consecutive traps is $\tau_m = L_u/\mu_{max}E_{av}$. These experimentally derived values are comparable to those obtained from the kinetic model based on the equilibrium partitioning theory and Kramer's rate theory:[30]

$$\tau_{trap} = \frac{\alpha N}{E_{av}^2 K} e^{-\varepsilon} \quad (2)$$

where α is the fitting parameter, K is the partition coefficient of the capillary−well array (Figure 3F), and $\varepsilon = \Delta W/k_BT$ is the reduced potential in which k_B is the Boltzmann's constant, T is the absolute temperature, and ΔW is the electrical potential energy drop in the translation of molecules over the entropic barrier along

the field direction. We further approximated ΔW as

$$\Delta W = NqE_w d_r \quad (3)$$

where q is the effective charge per base pair, 2.49×10^{-21} C/bp, E_w is the electric field strength within the wells, and $d_r = (Dt_w)^{1/2}$ is the transition region radius, which is equivalent to the characteristic diffusion length of molecules and is based on their diffusion coefficient,[31] $D \sim N^{-0.68}$, and the average time, $t_w = L_w/\mu_{max}E_{av}$, that they take to cross a well of length L_w. The optimal fitting parameter α across various field strengths was nearly constant at a standard deviation of $\pm$1.4% around a mean value of 8,300 V^2 s/(m^2 bp), which is comparable to 8684 V^2 s/(m^2 bp), the value reported for the sieving of a 100 bp DNA ladder in an 80 nm slit–well motif featuring the same pitch, 4 μm.[17]

The mean trapping time in the capillary–well array under E_{av} = 1000 V/cm increased with an increase in DNA length by up to tens of milliseconds as opposed to hundreds of milliseconds in the slit–well motif under E_{av} < 100 V/cm (Figure 3E). Here, this value dropped even further (<10 ms) when short DNA strands (<300 bp) and/or increased field strengths ($E_{av} \gtrsim$ 1500 V/cm) were used. The model adopted here shows excellent agreement with the experimental data and provides an insight into how the capillary–well motif, unlike a slit–well motif, maintains a near-equilibrium sieving mode under highly intense fields (>1000 V/cm) and thereby allows sieving that is more rapid than that obtained using a slit–well motif. Even under highly intense fields, the capillary–well design preserved selectivity, A, which can be restated as

$$A = \mu_{max}\alpha e^{-\varepsilon}/L_u E_{av} K \quad (4)$$

and thus it preserved the near-equilibrium sieving mode, partly because the partition coefficient K was low. Unlike a slit, a capillary limits the *configurational* freedom of strands to a quasi-1D space and thus reduces K and increases the entropic barrier $-k_BT$ ln K. Comparing the K values computed (Supporting Information) for the 70 nm capillary–well and 70 nm slit–well designs (Figure 3F), which are equivalent in all aspects but their entropic barriers, shows that the K value decreases with an increase in strand size more readily in the capillary–well motif than in the slit–well motif; the value for large strands (>300 bp) drops to a level that is smaller by about an order of magnitude. Most importantly, however, because of the term $\varepsilon = \Delta W/k_BT$, the drastic decline in A is curbed when E_{av} is increased, and the breakdown in the near-equilibrium sieving mode that is associated with a reduction in the A value is prevented; $\varepsilon \sim 1$ because capillaries, owing to their high restriction (resistance), limit E_w to an insignificant fraction of E_{av}, which ensures that $\Delta W \sim k_BT$. We determined that in a 70 nm capillary–well array featuring a pitch of 4 μm, E_w under E_{av} = 1000 V/cm was extremely low: it was ~0.3 V/cm as opposed to ~6.3 V/cm in an 80 nm slit–well array of the same pitch, under E_{av} = 26 V/cm. Such a low field inside the wells could also explain the presence of a distinctively high-voltage threshold for launching bands.

Sieving Proteins. We also tested whether quasi-equilibrium sieving (Ogston) of proteins can be achieved under highly intense driving fields. Proteins are clinically relevant molecules, and they are at the center of biomarker discovery.[32] An equimolar mixture of six sodium dodecyl sulfate (SDS)-denatured proteins, ranging in molecular weight from 11.4 to 340 kDa, was separated in a 70 nm capillary–well array featuring a pitch of 4 μm across a separation run of 3 cm (N_{trap} = 7500). As shown in Figure 4A, five out of the six proteins were rapidly resolved into distinct bands according to their molecular weights in <3 s after launching the mixture and after they had passed through ~100 traps within the first 400 μm run of the array (E_{av} = 1000 V/cm). Because ovalbumin and streptavidin are similar in size, they could not be resolved within such a short run; however, the two proteins were fully resolved toward the array end (Figure 4B). Based on the separation of these two proteins at a differential size of ΔM = 7.8 kDa and a resolution of R_s = 2.26, the minimum resolvable size difference was estimated to be R_M = 3.45 kDa. By comparison, all the remaining bands were detected at a higher resolution, ranging from 3.4 to 8.5, and with theoretical plate numbers of $1.1–2.6 \times 10^4$ (up to ~10^6 plates/m).

As in the sieving of short DNA strands, the launching of proteins within the array required a high-threshold field of E_{av} = 1000 V/cm; however, using this field, the six SDS–protein complexes were fully resolved when the 3 cm run was completed in an effective runtime slightly over 5 min. Small molecules migrated faster than large ones did and exhibited diminished field dependence in their mobility. Although the field dependence of their mobility varied, all proteins except ovalbumin and streptavidin were resolved into distinct bands in an effective runtime of roughly 2 min when the field was increased to E_{av} = 2000 V/cm (Figure 4B). This is unlike the separation observed in the case of short DNA molecules (Figure 3B) because the proteins passed through 50% more traps than the DNA molecules did and covered an additional 1 cm run. A plot of the molecular weight *versus* the logarithmic mobility of proteins separated under E_{av} = 1000 V/cm (Figure 4C) showed a linear trend (R^2 = 0.97) when the average values were obtained from separations performed under the same conditions (n = 5). The relative standard errors calculated for all six proteins were <3%, and thus the linearity further indicates that Ogston sieving was the mechanism underlying the high-field rapid sieving of proteins. By comparison, the sieving of proteins (20–120 kDa) in a 4 mm long self-assembled colloidal array of 160 nm silica particles, which was performed

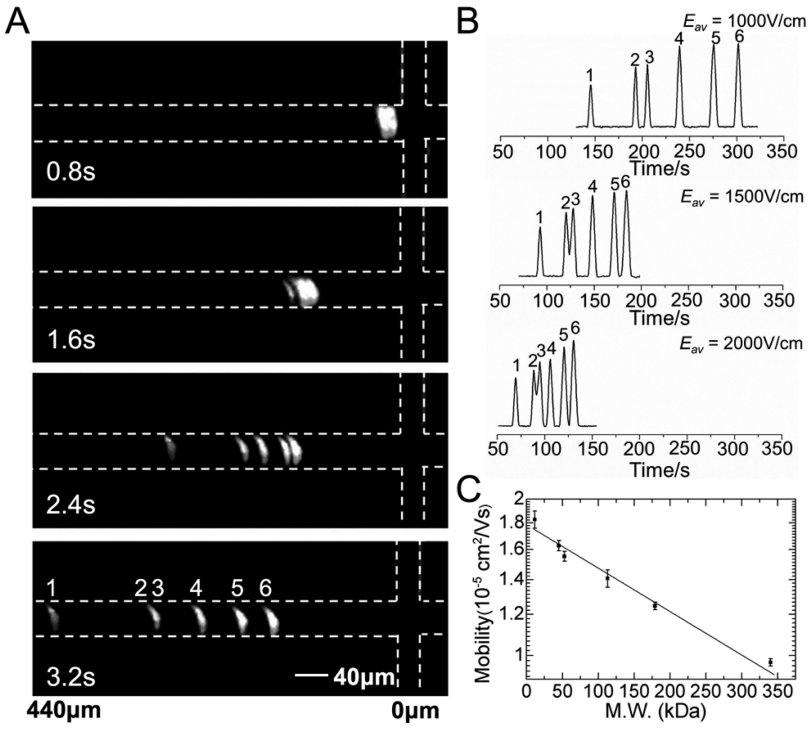

Figure 4. Electrophoretic separation of six SDS−protein complexes in a capillary−well motif (L_u = 4 μm; d_c = 70 nm; L_s = 3 cm); the band assignments are (1) cholera toxin subunit B (11.4 kDa), (2) ovalbumin (45 kDa), (3) streptavidin (52.8 kDa), (4) lectin GS-II (113 kDa), (5) human low-density lipoprotein (179 kDa), and (6) fibrinogen (340 kDa). Time-stamped fluorescent images (A) of the array near the sample-injection cross-junction showing baseline separation under E_{av} = 1000 V/cm. (B) Electropherograms obtained at the array end under various average field strengths. (C) Semilog plot of the apparent mobility of the SDS−protein complexes in the array under E_{av} = 1000 V/cm, shown against the molecular weight (MW) of proteins (n = 5).

under 30.9 V/cm, returned a comparable performance but took around 17 min.[11]

Sieving Long DNA. To evaluate the sieving of long DNA, we used molecules that covered a broad size range. An equimolar mixture of T4-DNA (166 kbp), λ-DNA (48.5 kbp), and *Eco*RI-cut λ-DNA fragments (6 fragments, 3530−21226 bp; radius of gyration, R_g, 109−345 nm) in 5× TBE buffer was fully resolved in slightly over 6 min in a 70 nm array (N_{trap} = 7500, L_u = 4 μm, L_s = 2 cm) under E_{av} = 1000 V/cm (Figure S1). This field was induced through a steady 2000 V directly applied across the entire sieve. Once again, when field strengths below 1000 V/cm were used, the launching of the samples failed, which suggests that the high-threshold electric field observed is independent of the molecule size and is instead an inherent characteristic of the array structure. Typical plate numbers were 2.4−3.9 × 10^4 (~10^6 plates/m). The resolution was 2.9 between 3.5 and 4.8 kbp chains but was as high as 5 between those >7 kbp. The chains of 4.8, 5.6, 5.8, and 7.4 kbp, being close in size, were resolved only slightly above baseline; the minimum resolvable size difference was estimated to be R_M = 182 bp based on the 5.6 and 5.8 kbp chains. These results compare favorably with those obtained from the 75 nm slit−well motif featuring a 4 μm pitch that was reported to be capable of sieving similarly sized DNA fragments through a 1.5 cm run in 30 min.[14]

To further investigate the mobility of long DNA chains, we conducted experiments in which a binary mixture of λ-DNA and T4-DNA was separated by using designs that featured distinct pitch sizes (4, 10, and 20 μm) and a 2 cm length under various E_{av}, ranging from 1000 to 2000 V/cm. At a given field strength, the runs were repeated five times using each design; the mobility mean and standard deviation values were obtained from electropherograms (Figure S2) and are compared in Figure 5A. Given the same field strength, T4-DNA migrated faster than λ-DNA did, and a comparable increase in the mobility of both chains was observed with an increase in the pitch size due to the reduction in the number of entropic traps. In all the designs, mobility under high fields (near 2000 V/cm) converged to 1.8 × 10^{-5} cm^2/Vs, as a result of which the two DNA chains lost their differential mobility.

In Figure 5A, the results show a strong agreement (R^2 > 0.97) with a simple scaling model:[13]

$$\mu = \frac{\mu_{max}}{1 + \alpha_1 \exp(\alpha_2/E_{av})} \quad (5)$$

where μ_{max}, α_1, and α_2 are treated as free parameters in least-squares fittings. The value of μ_{max}, the free-draining mobility, was nearly constant in all the curves (~2.25 × 10^{-5} cm^2/Vs). However, the parameters α_1 and α_2 varied from 1.8 to 8.6 × 10^{-2} and from 2000 to 4641 V/cm, respectively. The parameters α_1 and α_2 were

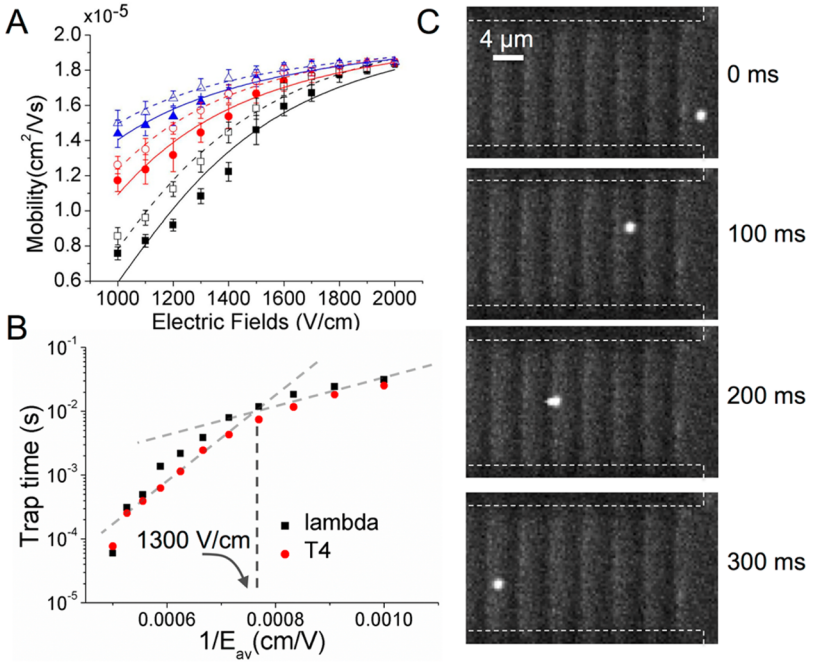

Figure 5. Electrophoretic separation of long DNA chains (λ and T4) in the capillary−well motif (d_c = 70 nm; L_s = 2 cm). (A) Mobility of λ-DNA (filled symbols) and T4-DNA (empty symbols) as a function of the field strength E_{av} (n = 5). The symbols denote sieve pitches of 4 μm (squares), 10 μm (circles), and 20 μm (triangles). Solid (λ-DNA) and dashed lines (T4-DNA) are the optimal fits obtained using eq 5. (B) Plot of ($1/E_{av}$) *vs* log(τ_{trap}). The dashed lines are drawn to guide the eye. (C) Time-stamped video frames showing a λ-DNA chain migrating through the array (L_u = 4 μm) under E_{av} = 1000 V/cm.

1−2 orders of magnitude larger than those measured for the slit−well motif; because α_1 compares the shortest trapping time possible to the drift time between two consecutive traps, our results suggest that, in the capillary−well motif, molecules spend a greater fraction of their drift time inside traps than they do when they are in the slit−well motif. When α_1 and α_2 are treated as free parameters, drawing conclusions regarding their trends is challenging. However, in the case of the 20 μm pitch sieve, α_2 varied only slightly (±10 V/cm) and the associated α_1 value provided a useful insight by suggesting that λ-DNA and T4-DNA spend roughly 8.2 and 6.4% of their drift time inside traps, respectively. T4-DNA is longer than λ-DNA, and thus it escaped from traps readily. In the slit−well motif, this was attributed to the escape probability of long chains being higher than that of short chains because the long chains contact a large opening area when escaping a slit.[13] However, when escaping from a capillary, long and short chains exceeding a certain size contact an equal opening area of the capillary, which implies that the escape probability of T4-DNA increases when it is packed in the form of dense blobs against capillary openings. Escape is then initiated by these densely packed blobs, and the remaining chain has no direct influence on the energy barrier height, which is represented in our model by α_2. Thus, α_2 is not expected to vary with the chain length, and it was an order of magnitude higher in the capillary−well motif than in the slit−well motif, which indicates that entropic barrier heights in the capillary−well motif were greater than those in the slit−well motif. When the energy barrier is increased, the tipping point of sieving shifts to driving fields of increased intensity.

The Boltzmann factor in eq 5 allocates a finite probability per unit time to DNA molecules for overcoming the energy barrier and, accordingly, identifies the relationship between log(τ_{trap}) and $1/E_{av}$ to be linear, featuring a slope of α_2. However, Figure 5B shows that the trapping time curves obtained based on the mobility data (Figure 5A) exhibit a piecewise linear relationship with a single change in slope (α_2), and that the curves are also independent of the pitch. In the case of λ-DNA and T4-DNA, the slopes of the segment immediately above the field threshold are 3695 and 4759 V/cm ($R^2 \sim 0.97$), respectively. These are comparable to the values calculated from the mobility data that were fitted using eq 5. However, the slope of the segment above ~1300 V/cm is higher than the aforementioned slopes in the case of both λ-DNA and T4-DNA, $\alpha_2 \sim$ 15000 V/cm ($R^2 > 0.99$, omitting the highest field applied), which indicates that the field begins to dominate the energy barriers and leaves the chains trapped each time for <10 ms. Even when intermediate fields were applied, the chains spent no more than 50 ms inside each trap, which can be observed in the sequence of video frames (Figure 5C) showing a λ-DNA chain migrating under 1000 V/cm. The chain jumps two energy barriers (dark regions) once every 100 ms and can be seen negotiating the fifth energy barrier in 200 ms. However, in the slit−well motif, the trapping time was typically on the order of seconds.[12] Moreover, in the slit−well motif, the escape

was captured in video frames depicting a single λ-DNA chain crossing a 10 μm long slit.[13] Capturing the escape here was a challenge (Figure 5C) as the chains crossed 10 μm long capillaries rapidly while accelerating under fairly high local fields (2000 V/cm). Nevertheless, the trapping and escape of both T4-DNA and λ-DNA chains were visualized utilizing a simplified design featuring a single set of 100 μm long capillaries 70 nm in diameter (Figure S3). These images further confirmed that a T4-DNA being larger than a λ-DNA spends comparatively less time when entering a capillary. The images also revealed that the chains upon entering the capillary assume an elongated state.

CONCLUSION

In summary, we demonstrated a facile method of constructing a highly efficient, robust sieve structure featuring an array of 70 nm diameter capillaries interleaved with wells, the capillary–well motif. The capillaries, owing to their confining nature, impose substantially greater entropic barriers on molecules than less resistive slits or pillars do at their onsets. Thus, driving molecules over these steep energy barriers requires electric fields much stronger than the usual fields, and this leads to an effective size-based separation of molecules. We also demonstrated that these steep entropic barriers preserve their resolving power over a broad range of increasing field strengths. Given this performance, and the unique fabrication process that is compatible with standard semiconductor manufacturing techniques, we expect that the capillary–well motif can bring integrated bioanalysis systems closer to reality.

MATERIALS AND METHODS

Microfabrication. A low-temperature oxide (LTO) layer was applied on silicon wafers covered with a 1 μm thick thermal oxide at a thickness of 5 μm by means of plasma-enhanced chemical vapor deposition and was used as a base on which the sieve structures were fabricated. Trenches, 2 μm wide and 2 μm deep, were formed on the LTO layer by using conventional photolithography and advanced oxide etching (AOE). Before depositing the doped glass, a thin (100 nm) film of silicon nitride (not shown in Figure 1) was introduced as a diffusion barrier. Next, we deposited a 5 μm thick layer of phosphorus-doped glass (phosphosilicate glass) by using a process of low-pressure CVD (LPCVD, 180 mTorr, 420 °C). As a result of the nonconformal step coverage profile exhibited by the layer, a single self-enclosed void extended within each trench, and then these voids were converted into 750 nm diameter cylindrical capillary tubes by using the reflow of the doped glass during a thermal annealing step (1000 °C, 1 h). The subsequent reflow steps required for scaling the diameter to <100 nm were conducted using rapid thermal annealing after the sample-injection cross-junction and wells had been structured. Specific wells spaced at 5 mm intervals along the array were further extended orthogonally to the array length to provide electrical access paths to the array through the electrodes placed in the respective reservoirs (Figure S4). This structuring of the dielectric layers was performed at a depth of 6 μm by means of AOE, which was used after conventional photolithography. Polydimethlysiloxane slabs were prepared with inlet/outlet ports and then permanently bonded over the sieve structures after surface activation was performed using oxygen plasma (29.6W Harrick Plasma, 45 s).

Reagents. Double-stranded DNA (dsDNA) molecules of various sizes, including a PCR 100 bp DNA ladder, DNA fragments from bacteriophage lambda *cI857 Sam7* (λ-DNA, 48 kbp), and a mixed digest of *Eco*RI-cut λ-DNA (3530–21226 bp), were obtained from Sigma-Aldrich. The bacteriophage T4 GT7 DNA (166 kbp) was purchased from Nippon Gene. To allow fluorescence-based detection, all the dsDNA samples were labeled with the bis-intercalating dye YOYO-1 (Life Technologies) at a dye/base pair ratio of 1:10 and prepared at a final concentration of 50 μg/mL in 5× TBE buffer (450 mM Tris/borate, 10 mM EDTA, pH 8.3) containing 4% v/v 2-mercaptoethanol and 1% v/v poly(vinylpyrrolidone) (MW = 10000), which were added to reduce photobleaching and suppress the electro-osmotic effect, respectively. To test the separation of denatured proteins, we obtained the following proteins in the form of Alexa Fluor 488 conjugates from Life Technologies: cholera toxin subunit B (11.4 kDa), ovalbumin (45 kDa), streptavidin (52.8 kDa), lectin GS-II (*Griffonia simplicifolia*, 113 kDa), human low-density lipoprotein (179 kDa), and fibrinogen (human plasma, 340 kDa). The proteins were mixed with 2 wt % SDS (Sigma-Aldrich) and 0.1 M dithiothreitol (Sigma-Aldrich) and then incubated in an 80 °C water bath for 10 min. After denaturation, the protein samples were diluted with 5× TBE buffer to a final concentration of 0.1 mg/mL.

Experiments. Each device was filled with the 5× TBE buffer. Electric fields were applied through platinum electrodes (Leego Precision Alloy) that were immersed in reservoirs and connected to a high-voltage power supply (Tianjin Dongwen Co. Ltd.) that was controlled using Labview (National Instruments). The separations reported for 2 cm long sieves at an average field of 1000 V/cm were realized by directly applying a steady 2000 V across the entire sieve. The separations at higher field strengths and/or using 3 cm long sieves were performed by applying 2000 V or lower across a distance of 1 cm at any given time so as to avoid dielectric breakdown. To sustain the migration of bands down the sieve, the potential was multiplexed to an array of electrodes placed along the length of the arrays at 5 mm intervals (Supporting Information text and Figure S4). During the tests, the device was observed under an epifluorescence microscope (Eclipse, Nikon) equipped with a solid-state laser at 488 nm and a filter cube set suitable for the excitation and detection of sample bands (ex/em 492/520 nm). Time-series images of single sample bands were captured using an EMCCD camera (iXon3 897, Andor) and analyzed using an image-processing software (ImageJ; NIH, Bethesda, MD) to generate electropherograms by extracting and plotting fluorescence intensities from regions of interest (~2 μm by 2 μm). Peaks were fitted with Gaussians, and the mean (maximal intensity) and the base width of each peak were determined. These values were subsequently used for assessing the resolution R_s between adjacent pairs of peaks (Supporting Information).

Conflict of Interest: The authors declare no competing financial interest.

Acknowledgment. This work was financially supported by the Research Grant Council of Hong Kong under Grant 621513.

Supporting Information Available: Additional materials related to the entropic sieving mechanism, the resolution benchmarking, the partition coefficient, and the sieving voltage as well as supporting tables and figures. This material is available free of charge *via* the Internet at http://pubs.acs.org.

REFERENCES AND NOTES

1. Han, J. Y.; Fu, J. P.; Schoch, R. B. Molecular Sieving Using Nanofilters: Past, Present and Future. *Lab Chip* **2008**, *8*, 23–33.

2. Slater, G. W.; Rousseau, J.; Noolandi, J.; Turmel, C.; Lalande, M. Quantitative Analysis of the Three Regimes of DNA Electrophoresis in Agarose Gels. *Biopolymers* **1988**, *27*, 509–524.
3. Dorfman, K. D. DNA Electrophoresis in Microfabricated Devices. *Rev. Mod. Phys.* **2010**, *82*, 2903–2947.
4. Volkmuth, W. D.; Austin, R. H. DNA Electrophoresis in Microlithographic Arrays. *Nature* **1992**, *358*, 600–602.
5. Huang, L. R.; Tegenfeldt, J. O.; Kraeft, J. J.; Sturm, J. C.; Austin, R. H.; Cox, E. C. A DNA Prism for High-Speed Continuous Fractionation of Large DNA Molecules. *Nat. Biotechnol.* **2002**, *20*, 1048–1051.
6. Bakajin, O.; Duke, T. A. J.; Tegenfeldt, J.; Chou, C. F.; Chan, S. S.; Austin, R. H.; Cox, E. C. Separation of 100-Kilobase DNA Molecules in 10 Seconds. *Anal. Chem.* **2001**, *73*, 6053–6056.
7. Duke, T. A. J.; Austin, R. H.; Cox, E. C.; Chan, S. S. Pulsed-Field Electrophoresis in Microlithographic Arrays. *Electrophoresis* **1996**, *17*, 1075–1079.
8. Turner, S. W.; Perez, A. M.; Lopez, A.; Craighead, H. G. Monolithic Nanofluid Sieving Structures for DNA Manipulation. *J. Vac. Sci. Technol., B* **1998**, *16*, 3835–3840.
9. Cabodi, M.; Turner, S. W. P.; Craighead, H. G. Entropic Recoil Separation of Long DNA Molecules. *Anal. Chem.* **2002**, *74*, 5169–5174.
10. Kaji, N.; Tezuka, Y.; Takamura, Y.; Ueda, M.; Nishimoto, T.; Nakanishi, H.; Horiike, Y.; Baba, Y. Separation of Long DNA Molecules by Quartz Nanopillar Chips under a Direct Current Electric Field. *Anal. Chem.* **2004**, *76*, 15–22.
11. Zeng, Y.; Harrison, D. J. Self-Assembled Colloidal Arrays as Three-Dimensional Nanofluidic Sieves for Separation of Biomolecules on Microchips. *Anal. Chem.* **2007**, *79*, 2289–2295.
12. Han, J. Y.; Craighead, H. G. Entropic Trapping and Sieving of Long DNA Molecules in a Nanofluidic Channel. *J. Vac. Sci. Technol., A* **1999**, *17*, 2142–2147.
13. Han, J. Y.; Turner, S. W.; Craighead, H. G. Entropic Trapping and Escape of Long DNA Molecules at Submicron Size Constriction. *Phys. Rev. Lett.* **1999**, *83*, 1688–1691.
14. Han, J. Y.; Craighead, H. G. Separation of Long DNA Molecules in a Microfabricated Entropic Trap Array. *Science* **2000**, *288*, 1026–1029.
15. Han, J. Y.; Craighead, H. G. Characterization and Optimization of an Entropic Trap for DNA Separation. *Anal. Chem.* **2002**, *74*, 394–401.
16. Fu, J. P.; Mao, P.; Han, J. Y. Nanofilter Array Chip for Fast Gel-Free Biomolecule Separation. *Appl. Phys. Lett.* **2005**, *87*, 263902.
17. Fu, J. P.; Yoo, J.; Han, J. Y. Molecular Sieving in Periodic Free-Energy Landscapes Created by Patterned Nanofilter Arrays. *Phys. Rev. Lett.* **2006**, *97*, 018103.
18. Dorfman, K. D.; King, S. B.; Olson, D. W.; Thomas, J. D. P.; Tree, D. R. Beyond Gel Electrophoresis: Microfluidic Separations, Fluorescence Burst Analysis, and DNA Stretching. *Chem. Rev.* **2013**, *113*, 2584–2667.
19. Ong, W. L.; Tang, K. C.; Agarwal, A.; Nagarajan, R.; Luo, L. W.; Yobas, L. Microfluidic Integration of Substantially Round Glass Capillaries for Lateral Patch Clamping on Chip. *Lab Chip* **2007**, *7*, 1357–1366.
20. Cao, Z.; Ren, K. N.; Wu, H. K.; Yobas, L. Monolithic Integration of Fine Cylindrical Glass Microcapillaries on Silicon for Electrophoretic Separation of Biomolecules. *Biomicrofluidics* **2012**, *6*, 036501.
21. Cao, Z.; Yobas, L. Fast DNA Sieving through Submicrometer Cylindrical Glass Capillary Matrix. *Anal. Chem.* **2014**, *86*, 737–743.
22. Liu, Y. F.; Yobas, L. Cylindrical Glass Nanocapillaries Patterned *via* Coarse Lithography (> 1 μm) for Biomicrofluidic Applications. *Biomicrofluidics* **2012**, *6*, 046502.
23. Cao, H.; Tegenfeldt, J. O.; Austin, R. H.; Chou, S. Y. Gradient Nanostructures for Interfacing Microfluidics and Nanofluidics. *Appl. Phys. Lett.* **2002**, *81*, 3058.
24. Li, W.; Tegenfeldt, J. O.; Chen, L.; Austin, R. H.; Chou, S. Y.; Kohl, P. A.; Krotine, J.; Sturm, J. C. Sacrificial Polymers for Nanofluidic Channels in Biological Applications. *Nanotechnology* **2003**, *14*, 578.
25. Guo, L. J.; Cheng, X.; Chou, C. F. Fabrication of Size-Controllable Nanofluidic Channels by Nanoimprinting and Its Application for DNA Stretching. *Nano Lett.* **2004**, *4*, 69–73.
26. Liang, X. G.; Morton, K. J.; Austin, R. H.; Chou, S. Y. Single Sub-20 nm Wide, Centimeter-Long Nanofluidic Channel Fabricated by Novel Nanoimprint Mold Fabrication and Direct Imprinting. *Nano Lett.* **2007**, *7*, 3774–3780.
27. Xia, Q. F.; Morton, K. J.; Austin, R. H.; Chou, S. Y. Sub-10 nm Self-Enclosed Self-Limited Nanofluidic Channel Arrays. *Nano Lett.* **2008**, *8*, 3830–3833.
28. Xia, D. Y.; Gamble, T. C.; Mendoza, E. A.; Koch, S. J.; He, X.; Lopez, G. P.; Brueck, S. R. J. DNA Transport in Hierarchically-Structured Colloidal-Nanoparticle Porous-Wall Nanochannels. *Nano Lett.* **2008**, *8*, 1610–1618.
29. Menard, L. D.; Ramsey, J. M. Fabrication of Sub-5 nm Nanochannels in Insulating Substrates Using Focused Ion Beam Milling. *Nano Lett.* **2011**, *11*, 512–517.
30. Stockmayer, W. H. In *Molecular Fluids*; Balian, R., Weill, G., Eds.; Gordon and Breach Science Publishers: Langhorne, PA, 1976.
31. Nkodo, A. E.; Garnier, J. M.; Tinland, B.; Ren, H. J.; Desruisseaux, C.; McCormick, L. C.; Drouin, G.; Slater, G. W. Diffusion Coefficient of DNA Molecules during Free Solution Electrophoresis. *Electrophoresis* **2001**, *22*, 2424–2432.
32. Sleno, L.; Emili, A. Proteomic Methods for Drug Target Discovery. *Curr. Opin. Chem. Biol.* **2008**, *12*, 46–54.